ORIGINAL PAPER

Meso-Cenozoic extensional structures in the Northern Tarim Basin, NW China

Yue-Jun Li · Yan Zhao · Long-De Sun ·
Wen-Jie Song · Duo-Ming Zheng · Ya-Lei Liu ·
Dao-Xuan Wang · Jian-Feng Hu · Qi-Rui Zhang

Abstract Meso-Cenozoic extensional structures are important for understanding the tectonics of the Chinese Central Asia. This paper presents a systematic investigation on the Meso-Cenozoic extensional structures in the Northern Tarim Basin. Close interpretations of seismic data reveal that the Meso-Cenozoic extensional structures were widely developed in the Northern Tarim Basin. These extensional structures are regionally composed of many small normal faults, which usually group into left- or right-step en echelon and form several transtensional fault zones. Combinations of normal faults in profile become small graben-horst or staircase-like cross-sections. Based on the areal distribution, structural style, combination relationship, formation and evolution time, and formation mechanism of the extensional structures, we found that the Meso-Cenozoic extensional structures in Northern Tarim Basin can be classified into two conjugate normal fault systems, which were formed separately in Jurassic-Early Cretaceous and Late Cretaceous-Neogene. The former is likely associated with the stress relaxation after a collisional orogeny accompanied with a certain degree of anticlockwise rotation of the Tarim block relative to the South Tianshan; the latter is possibly induced by the east by south tectonic escape of the Tarim block with a certain degree of clockwise rotation relative to the South Tianshan triggered by the far-field effect of the Himalayan orogeny.

Y.-J. Li · Y. Zhao · Y.-L. Liu · Q.-R. Zhang (✉)
Institute of Geology and Geophysics, Chinese
Academy of Sciences, Beijing 100029, China
e-mail: qrzhang@mail.iggcas.ac.cn

L.-D. Sun
PetroChina Company Limited, 9 Dongzhimen North Street,
Dongcheng District, Beijing 100007, China

W.-J. Song · D.-M. Zheng · J.-F. Hu
Tarim Oil-field Company, PetroChina,
Korla, Xinjiang 841000, China

D.-X. Wang
Hefei University of Technology, Tunxi Road,
Hefei, Anhui 230009, China

Introduction

Tarim Basin is one of the large Meso-Cenozoic hydrocarbon-bearing basins in Central Asia (Fig. 1). The whole Central Asia including the Tarim block was in the Late Cenozoic regional strong compressional tectonic regime controlled by the far-field effect of the Himalayan orogeny (Guo et al. 1992; Sobel and Dumitru 1997; Li et al. 2001b). Compressional tectonics abnormally developed with scarce extensional structures. Typical compressional thrust structures developed in the Late Cenozoic orogenic thrust belt in the periphery of the Tarim Basin (Allen et al. 1999; Scharer et al. 2004; Lu et al. 1994, 2000; Liu et al. 2000; Chen et al. 1998; Jia et al. 1997; Li et al. 2001b, 2008; Sun et al. 2002; Yang et al. 2010; Zheng et al. 2007; Tang et al. 2004; Wang et al. 2002, 2009). The orogenic belts surrounding the Tarim Basin, either developed during the collisional orogenic period in Paleozoic or the mountain building stage in Late Cenozoic, were all created under regional compressional tectonic background, and thus compressional thrust structures are dominant and became the focus of attention (Sobel and Dumitru 1997; Yin et al. 1998;
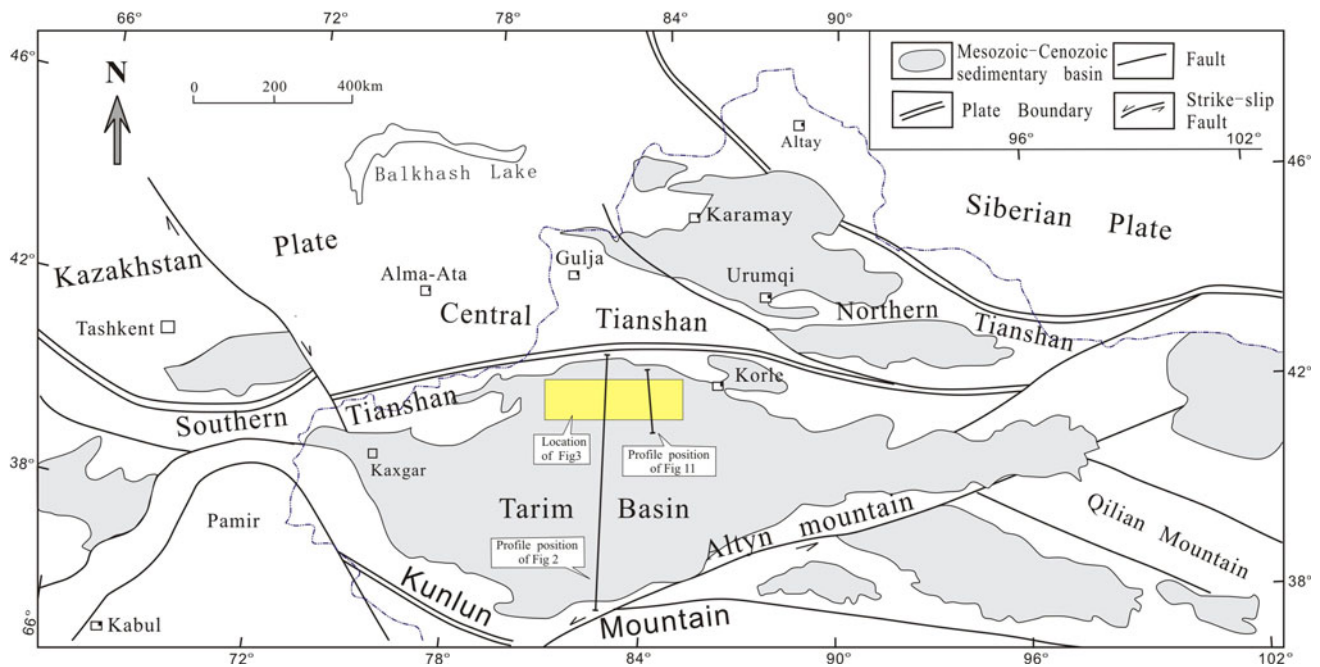
Fig. 1 Tectonic framework of the Tarim Basin and its vicinity

Bullen et al. 2001; Li et al. 2009, 2010; Zhang et al. 1996). Investigations on structural deformation within the Tarim Basin are also focused on the compressional thrust structures (Zheng et al. 2009; Meng et al. 2008). Few Meso-Cenozoic extensional structures have been investigated in the study area, in spite of some early studies on Meso-Cenozoic extensional structures along the Yaha and Luntai fault zones (1 and 2 in Fig. 3) (Tang et al. 1999; Tang and Jin 2000; Wei et al. 2001). This paper presents a systematic investigation on the Meso-Cenozoic extensional structures in the Northern Tarim Basin.

Northern Tarim Basin is hydrocarbon-rich with several important oil and gas accumulations (Figs. 1, 2, 3). With the extensive oil and gas exploration, the improving precision of seismic data, and especially the constantly increasing of the 3D seismic coverage area, we are able to characterize more finely the structural deformations within the basin.

Careful interpretation of the seismic data discovers the extensive development of the Meso-Cenozoic extensional structures in the Northern Tarim Basin (Figs. 1, 2, 3). A large number of small normal faults arrange in left- or right-step en echelon and can be grouped into four sets of transtensional fault zones (Figs. 3 and 10), and further combined into two conjugate normal fault systems (Fig. 10). This paper will depict the features of the Meso-Cenozoic extensional structures in the Northern Tarim Basin and discuss their formation and evolution, as well as their formation mechanism.

Generations of the Meso-Cenozoic extensional structures in the Northern Tarim Basin

Table 1 is a concise (seismic) stratigraphic chart of the Northern Tarim Basin. It is a basic stratigraphic criterion for the interpretation of seismic data and description of the Meso-Cenozoic extensional structures. Correlations of important seismic reflection surfaces with lithostratigraphic units and chronostratigraphic units in the table are based on Jia et al. (1992, 2004) and Wang (1992).

In Northern Tarim Basin, the well-developed Meso-Cenozoic normal faults usually are in en echelon and gather into transtensional fault zones (Fig. 3). As shown in profile, they form graben-horst or staircase-like cross-sections. Below some of the normal fault zones, there are large faults (for example the Yaha and Luntai faults; see Fig. 3), which indicate that the structural development in Meso-Cenozoic was specifically intensified by the preexisting fault structures. However, the development of normal faults is not confined to the areas having deep fault structures. A large number of Meso-Cenozoic normal faults did develop in areas with no preexisting deep faults (such as areas to the south of Sangtamu Oilfield) (Fig. 3). Our results show that there are two generations/stages of Meso-Cenozoic extensional structural development in the Northern Tarim Basin. The first stage is from the Jurassic to Early Cretaceous (colored blue in Fig. 3), occurred mainly in the eastern part of Lunnan Lower Uplift (I1 in Fig. 3). The second is from the Late Cretaceous to
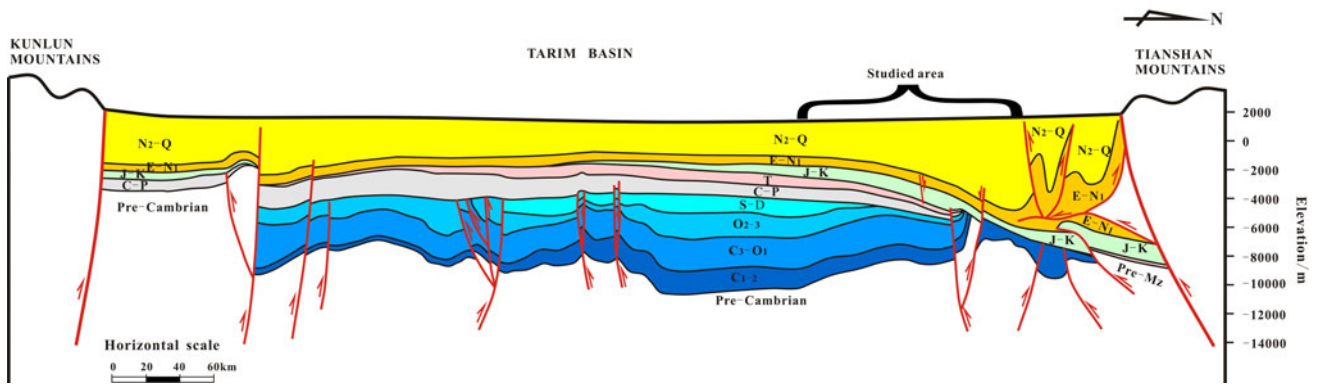
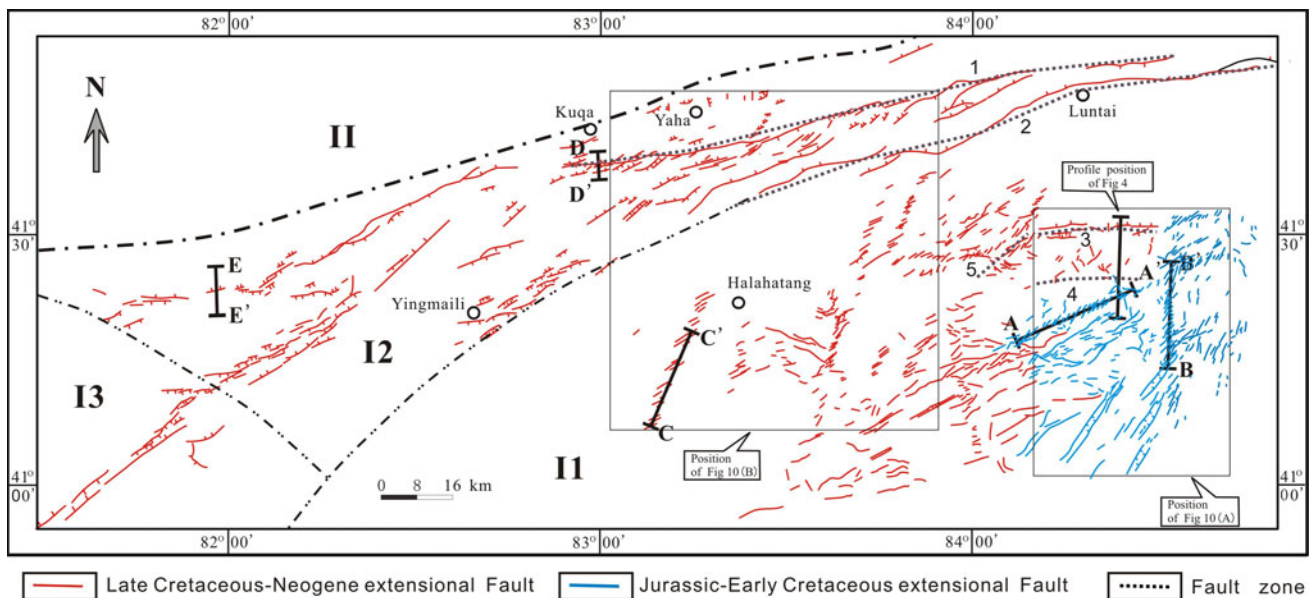**Fig. 2** A geologic section crossing the Tarim Basin from north to south

Fig. 3 Distribution of normal fault zones in the Tabei Rise: *1* Tabei Rise; *I1* Lunnan Lower Uplift; *I2* Luntai Uplift; *I3* Yingmaili Lower Uplift; *II*-Kuqa Depression. Normal faults of the Jurassic-Early

Cretaceous stage are shown in *blue color* and the Late Cretaceous-Neogene stage in *red color*. The names of fault zones are: *1* Yaha; *2* Luntai; *3* Lunnan; *4* Sangtamu; *5* Lunxi

Early-Middle Neogene (colored red in Fig. 3), developed in the western and northern parts of Tabei Rise (I2 and I3 in Fig. 3) and with minor influence in the eastern part of Lunnan Lower Uplift.

Post-Triassic Meso-Cenozoic extensional structures in the Northern Tarim Basin

In Northern Tarim Basin, the contact between Meso-Cenozoic and pre-Mesozoic is an important unconformity with varying stratigraphic hiatus. The Permian magmatism brought further an uneven surface to the top of Permian (Tg in Table 1). All these factors prevent us to determine the initiation time of the Meso-Cenozoic extensional structures from the seismic profiles. Therefore, the definition of the onset of extension has to depend on the investigation of the

closely related thrust structures, which were certainly formed earlier than the onset of extension.

In Lunnan region, there are three fault zones, namely the Lunnan, Sangtamu, and Lunxi (3, 4, and 5 in Fig. 3). They are capable of providing distinct records of thrusting event. The Sangtamu fault zone (Fig. 4) records especially the initiation of thrusting at the terminal Permian–Early Triassic.

The 3D seismic profile crossing the Sangtamu fault zone (Fig. 4) shows that the fault zone comprises two faults: one on the north and the other on the south. Under the control of the thrusting of the two faults, the strata between them were folded into anticlines. The fault displacements are large below the Tg reflection surface (Fig. 4b), but small above and even too small to be recognized where only folding can be seen. The amplitudes of anticlines below the

Table 1 Concise (seismic) stratigraphic chart of Tabei Rise, Tarim Basin (modified after Jia et al. 1992, 2004; Wang 1992)

Chronostratigraphic unit			Lithostratigraphic unit		Code number of seismic reflection surface
Quaternary (Q)			Xiyu Fm		T2
			Kuqa Fm		
Neogene (N)	Pliocene (N2)				T3
	Miocene (N1)		Kangcun Fm		T5
			Jidik Fm		T6
Paleogene (E)	Oligocene (E3)		Suviyi Fm		T7
	Eocene (E2)		Kumglim Fm		
	Paleocene (E1)				T8
Cretaceous (K)	Upper (K2)		Gucheng Fm		
	Lower (K1)		Bashijilik Fm		
			Kapushaliang Group	Baxigai Fm	
				Shushanhe Fm	
				Yageliemu Fm	T8-2
Jurassic (J)	Upper (J3)		Karaza Fm		
			Qigu Fm		
	Middle (J2)		Qakmak Fm		
			Kezilenul Fm		
	Lower(J1)		Yangxia Fm		
			Ahe Fm		T8-3
Triassic (T)	Upper (T3)		Taliqike Fm		
			Huangshanjie Fm		
	Middle (T2)		Kelamayi Fm		
	Lower (T1)		Ehuobulake Fm		Tg
Permian (P)	Lopingian (P3)		Shajingzi Fm		
	Guadalupian (P2)		Kaipaizileike Fm		
	Cisuralian (P1)		Kupukuziman Fm		
			Nanzha Fm		Tg2
Carboniferous (C)	Pennsylvanian (C2)		Xiaohaizi Fm		
			Karashayi Fm		
	Mississippian (C1)		Bachu Fm		
			Donghetang Fm		Tg3
Devonian					Tg4
Silurian					Tg5
Ordovician					Tg6
Cambrian					Tg8
Precambrian					

Tg surface are obviously larger than those above the Tg surface. The Paleozoic anticlines are consistent and have larger amplitudes, whereas the kernels of anticlines display obvious erosion and absence of many strata. The amplitudes of anticlines above the Tg surface decrease gradually and finally disappear at the top of Triassic, T8-3 (Fig. 4b).

Therefore, it is evident that the Sangtamu fault zone as well as its associated anticlines were active in the terminal Permian–Early Triassic and the thrusting ceased at the end of Triassic.

According to the evolution of Sangtamu fault zone, it is likely that the tectonic regime of the Northern
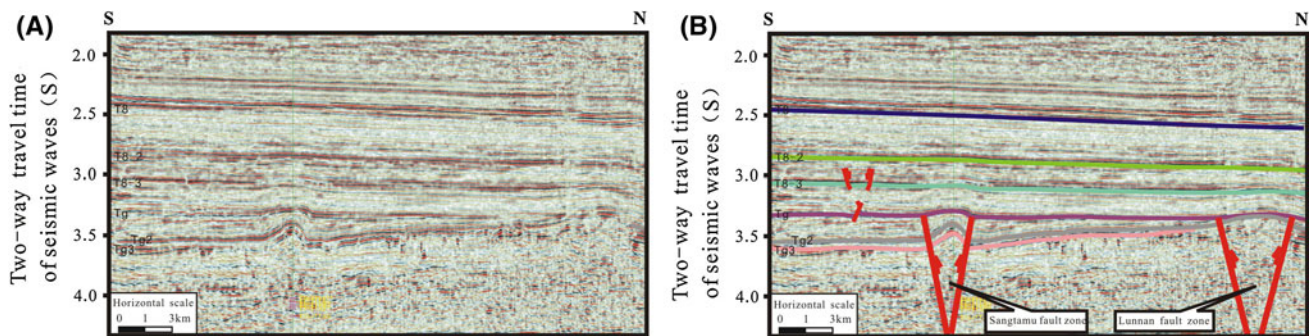
Fig. 4 The N–S trending 3D seismic profile crossing the Sangtamu and Lunnan fault zones: **a** original and **b** interpreted (location of the profile shown in Fig. 3; code number of seismic reflection surface shown in Table 1)
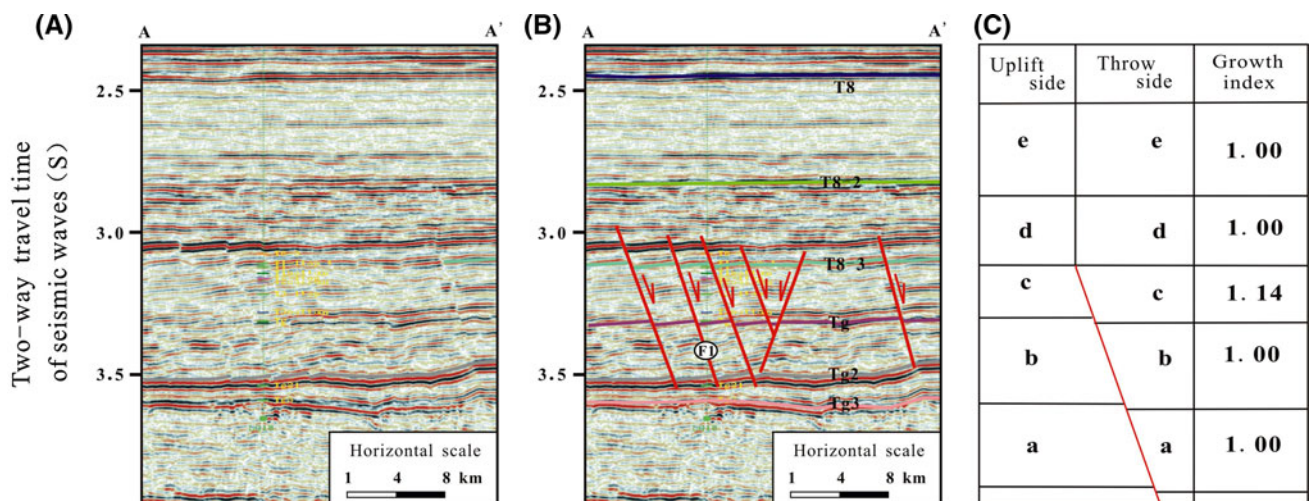

Fig. 5 A–A′ seismic profile in the Lunnan Lower Uplift: **a** original, **b** interpreted, **c** growth indices of the F1 fault: *a* Upper Permian; *b* Triassic; *c* Lower Jurassic; *d* Middle and Upper Jurassic; *e* Cretaceous (location of the profile shown in Fig. 3; code number of reflection surface shown in Table 1)
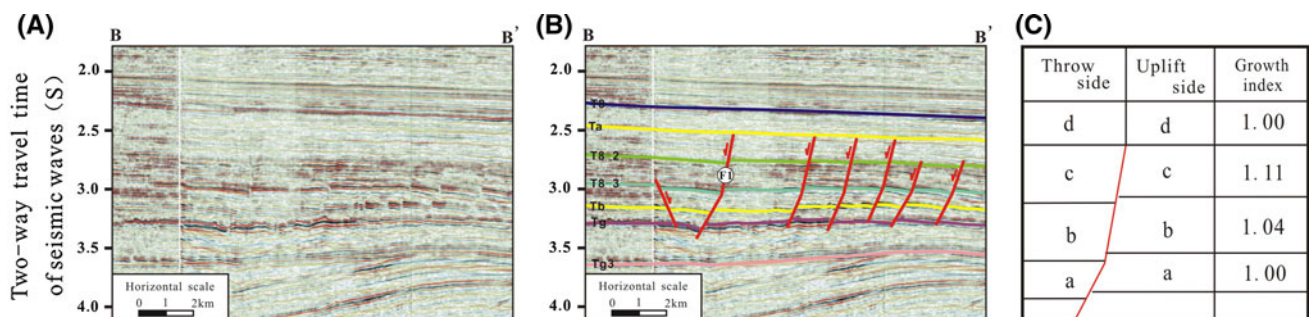

Fig. 6 B–B′ seismic profile in the eastern side of the Lunnan Lower Uplift: **a** original, **b** interpreted, and **c** growth indices of F1 fault: *a* Upper Triassic; *b* Jurassic; *c* Lower Cretaceous; *d* Upper Cretaceous. In **b,** Ta surface is the highest stratigraphic level being disconnected; Tb is the surface selected within Triassic for the calculation of growth indices (location of the profile shown in Fig. 3; code number of reflection surface shown in Table 1)

Tarim Basin during the terminal Permian–Triassic was compressional. The typical structural deformations are represented by thrust faults and related folds, and the Meso-Cenozoic extensional structures are likely formed after the Triassic.

Jurassic-Early Cretaceous extensional structures

The Jurassic-Early Cretaceous normal faults are mainly seen in the eastern part of Lunnan Lower Uplift (I1 in Fig. 3) and are rare on the Luntai Uplift (I2 in Fig. 3).

A–A′ cross-section is an ENE trending 3D seismic profile located in a Meso-Cenozoic normal fault zone (Figs. 3, 5). The normal fault zone comprises regionally a series of small normal faults, which arrange in right-step en echelon and constitute a left-lateral transtensional fault zone. In profile, several normal faults with similar dip direction show staircase-like sections and those with different dip directions constitute small graben-horst structures. The disconnections of normal faults extend upward into the lower part of Jurassic and downward into Carboniferous. The faults clearly cut the base of the Permian (Tg2) and intrude into the Carboniferous (Fig. 5b), where the fault displacements quickly decrease and disappear. Some faults are thrust faults in the lower part but normal faults in the upper part (see the fault in the right most of Fig. 5b). This phenomenon indicates that early thrusting may occur.

In order to reveal the evolution of a fault from a seismic profile, the growth index method (Tang and Jin 2000; Wei et al. 2001) is used. The index is commonly used in describing the formation and evolution of a fault, especially a normal fault, when the stratigraphic units on both sides of the fault did not experience erosion after deposition. The growth index is a ratio of the thickness of stratigraphic unit on the throw side to that of the uplift side. The equation of the growth index is

$$Ei = H1/H2.$$

Here, Ei is the growth index, $H1$ the thickness of a stratigraphic unit on the throw side, and $H2$ the thickness of the same stratigraphic unit on the uplift side. If $Ei = 1$, the thicknesses of a stratigraphic unit on the two sides of a fault are equal and signify that during the deposition of the stratigraphic unit the fault was not active. When $Ei > 1$, the thickness of a stratigraphic unit on the throw side is larger than that on the uplift side and reveals that the fault was active during the deposition of the stratigraphic unit. The larger the value of Ei is, the stronger the activity of the fault becomes.

In order to study the evolution of the faults in A–A′ seismic profile, growth indices of F1 fault were calculated (Fig. 5c). The probable existence of the Permian–Triassic thrust structures is outside the scope of this paper and is not considered here. The fault throws of the top and bottom of the Triassic on the two sides of the fault are the same; therefore, the thicknesses of Triassic on the two sides of the fault are equal (a and b in Fig. 5c) and the growth index is 1.00, indicating that the normal fault was not active in the Triassic. In Lower Jurassic, the difference in strata thicknesses between two sides of the fault is obvious and the thickness on the throw side is obviously larger than that on the uplift side and the growth

index is 1.14 (c in Fig. 5c). The fault does not cut the Middle-Upper Jurassic and strata above (d and e in Fig. 5c), and the growth index is 1.00. These indices indicate that the fault zone occurred at Early Jurassic and stabilized quickly with a short evolution and is typically representative of the Jurassic extensional structures in the Tabei region.

The occurrence of this normal fault zone is likely one of the most reliable evidences of the Jurassic extensional structures in the study area.

B–B′ profile is a nearly N–S trending 3D seismic profile in the eastern part of the Lunnan Lower Uplift (I1 in Fig. 3). Along the profile, there are many small normal faults, which arrange in left-step en echelon and constitute a nearly N–S trending right-lateral transtensional fault zone (Figs. 3, 6).

The normal faults cut downward into the Paleozoic through Tg reflection surface and become unclear (Fig. 6b). Upwardly, they cut the Middle Cretaceous, but do not affect the Upper Cretaceous. The dip angle of the faults changes near the T8-3 reflection surface, steeper above and gentler below (Fig. 6b), and is likely resulted from a kind of fault refraction due to the lithological variation. Drilling data in the area show that rocks of the Jurassic are mainly sandstone and those of the Triassic are mostly mudstone. The Triassic rocks are relatively softer than the Jurassic rocks and this is likely the cause of the changes of dip angle of faults near T8-3. The F1 fault and the fault on its left side (Fig. 6b) constitute a small graben, whereas F1 and faults on its right side form staircase-like fault group. In order to analyze the fault evolution, growth indices of F1 are calculated (Fig. 6c).

Growth index of the Upper Triassic (a in Fig. 6c) is 1.00, indicating that the normal fault was not active. However, growth index of the Jurassic (b in Fig. 6c) is 1.04, signifying the onset of the normal faulting. The growth index 1.11 of the Lower Cretaceous (c in Fig. 6c) is the largest, representing the faulting entered the peak stage of extension. However, the Upper Cretaceous (d in Fig. 6c) was not influenced by the faulting since the growth index is 1.00, suggesting that the faulting had ceased.

The formation times of the normal faults in B–B′ and A–A′ profiles are the same at the Jurassic, but the duration of the faulting in B–B′ profile is longer. They are likely the fault structures formed in the same period and under an identical structural stress field.

In the later of this extensional stage, the influence of the extension extended to the Luntai Uplift (I2 in Fig. 3), since in the Yaha fault zone occur not only the Late Cretaceous-Neogene extensional structures but also the Early Cretaceous extensional structures (as shown in D–D′ profile in Fig. 7, see text below).
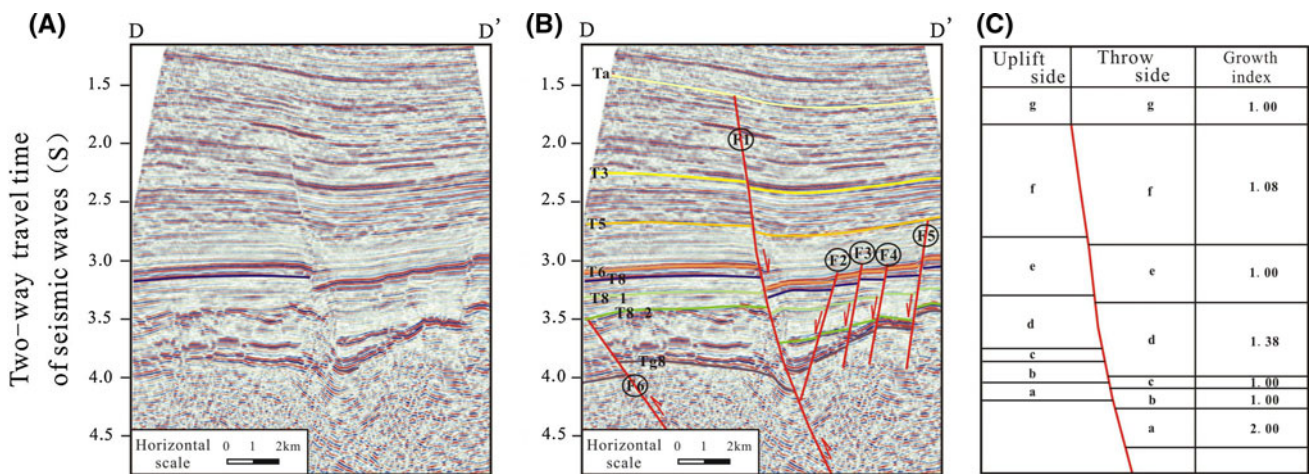
Fig. 7 D–D′ seismic profile crossing the Yaha fault zone: **a** original, **b** interpreted, and **c** growth indices of F1 fault: *a* Kapushaliang Group; *b* Bashijiqike Formation-Gucheng Formation; *c* Kumglim Formation-Suviyi Formation; *d* Jidik Formation; *e* Kangcun Formation; *f* Lower-Middle Kuqa Formation; *g* Upper Kuqa Formation and Quaternary (location of the profile shown in Fig. 3; code number of reflection surface shown in Table 1)

Late Cretaceous-Neogene extensional structures

Late Cretaceous-Neogene extensional structures are widely developed in the midwestern and northern parts of the Tabei Rise (I in Fig. 3), and the Meso-Cenozoic extensional structures along the Yaha and Luntai fault zones (1 and 2 in Fig. 3) were recognized more than 10 years ago, because they are large (the fault displacements are up to hundred meters) (Tang et al. 1999; Tang and Jin 2000; Wei et al. 2001). New and high precision seismic exploration data, especially the 3D seismic exploration data, reveal that the Late Cretaceous-Neogene normal faults are widely distributed in the Tabei Rise and not confined to the Yaha and Luntai fault zones. The Meso-Cenozoic normal faults developed along the Yaha fault zone are resulted from two extensional stages: the Early Cretaceous normal fault activity likely belongs to the Jurassic-Early Cretaceous stage and the two Neogene normal fault activities are related to the Late Cretaceous-Neogene stage.

D–D′ profile (Figs. 3, 7) is a nearly N–S trending 3D seismic profile crossing the Yaha fault zone. In profile, F1 is the major fault (Fig. 7b), F2–F5 are likely the faults derived in the later stage of the Yaha faulting, and F6 is a sub-fault associated with the early thrusting stage of the Yaha faulting (Fig. 7b). The Meso-Cenozoic normal faults along the Yaha fault zone constitute generally a small graben. From the seismic profile, the Cretaceous (T8-2 in Table 1) overlies unconformably on the Lower Paleozoic and even Precambrian (Tg8), highlighting the great sedimentary gap between them (Fig. 7b). The major fault F1 exhibits thrust feature below the Cretaceous, but above the Cretaceous, it converts to normal fault. Collectively, F1 assumes the characteristics of a negative reversal structure. The bases of Paleozoic on the two sides of the fault are very close to each other, suggesting that the early thrusting was almost completely reversed (Fig. 7b).

The sub-fault F6 formed in the same time as the early thrusting of F1 (Fig. 7b) but was later stabilized and not
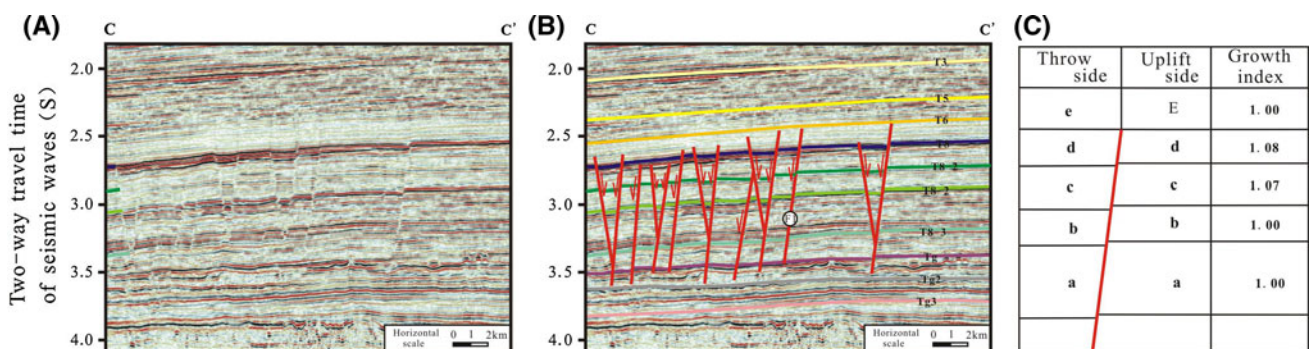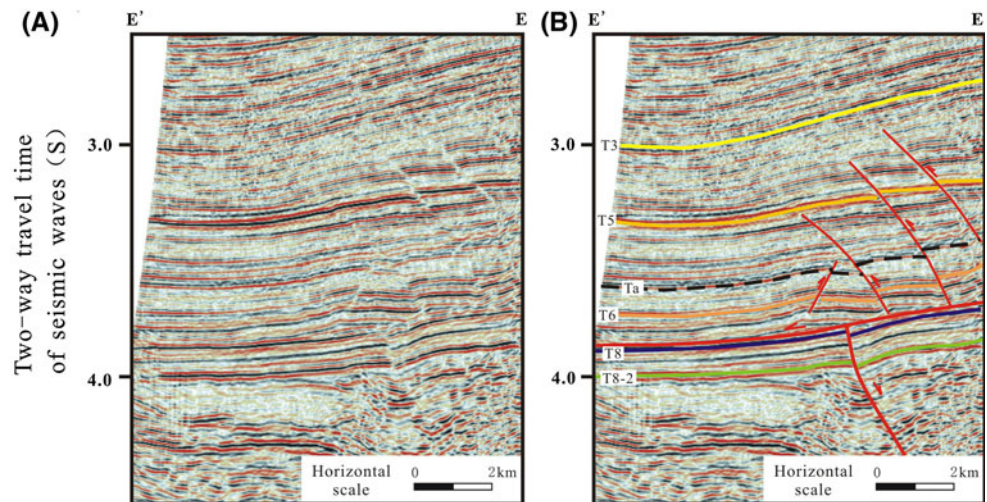

Fig. 8 C–C′ seismic profile in the western Lunnan Lower Uplift: **a** original, **b** interpreted, and **c** the growth index of F1 fault: *a* Jurassic; *b* Lower Cretaceous; *c* Upper Cretaceous; *d* Paleogene; *e* Neogene and strata above (location of the profile shown in Fig. 3; code number of reflection surface shown in Table 1)

being negatively reversed. This convincingly proves the existence of the early thrusting. Based on F1, the growth indices of the Meso-Cenozoic normal faults will be calculated and the evolution discussed.

The Cretaceous covered directly and unconformably on the Cambrian with a great stratigraphic gap between them. Before the deposition of the Cretaceous, the study region remained in a prolonged uplift-erosion period and the fault extension did not occur. In the Early Cretaceous, the thicknesses of the Kapushaliang Group on the two sides of the Yaha fault differ greatly (Fig. 7b): the thickness in the throw side is twice the thickness in the uplift side and the growth index is 2.00 (a in Fig. 7c), highlighting the inception of the extension. Later on, the thicknesses of Bashijiqike Formation-Gucheng Formation of Middle-Late Cretaceous (b in Fig. 7c) and Kumglim Formation-Suviyi Formation of Paleogene (c in Fig. 7c) on the two sides of the fault are identical with growth index 1.00, signifying the faulting ceased. During the deposition of the Neogene Jidik Formation (d in Fig. 7c), the Yaha fault extended once again with a growth index of 1.38. During the deposition of the Kangcun Formation, the Yaha faulting stopped again with a growth index of 1.00 (e in Fig. 7c). Until the deposition of the middle-lower Kuqa Formation (f in Fig. 7c), the third extension of the Yaha fault happened and the growth index is 1.08.

The first extension of the Yaha fault, corresponding to the normal faulting during the deposition of the Early Cretaceous Kapushaliang Formation, produced the Jurassic-Early Cretaceous extensional structures. The second extension, including the normal faultings happened during the deposition of Jidik Formation and Middle-Lower Kuqa Formation, affiliates to the Late Cretaceous-Neogene extensional structures.

C–C′ profile is a 3D seismic profile trending NE–SW in the Halahatang region in the west of Lunnan Lower Uplift

(I1 in Figs. 3, 8). The regional distribution of the small normal faults is left-step en echelon and forms a NNE trending right-lateral transtensional fault zone (Fig. 3), and in profile form a series of small graben-horst structures (Fig. 8b). The normal faults downwardly pass through the Tg surface and become unclear after entering Permian. Upwardly, they disconnect the T8 surface and enter the Paleogene, and at most, may reach the base of the Neogene (T6 in Fig. 8b). The growth indices calculated from the F1 fault (Fig. 8b) are used to reveal the evolution of the normal faults.

The Jurassic and Lower Cretaceous on the two sides of F1 are equal in thickness (a and b in Fig. 8c) with a growth index of 1.00, indicating that the extension did not happen at that time. From the Upper Cretaceous upward, difference between the strata thicknesses on the two sides of the fault appears (c in Fig. 8c) and the growth index is 1.07, showing that the extension had started since the Early Cretaceous. The extension persisted up till the Paleogene, since the strata thicknesses on the two sides of the fault are different and have a growth index of 1.08 (d in Fig. 8c). The fault upwardly disconnects strata up till T6 (Fig. 8c), and after disconnecting Paleogene, it does not cut the Neogene and the strata above; therefore, the growth index of Neogene and strata above is 1.00 (e in Fig. 8c), signifying the ending of the extension.

Late Cretaceous-Neogene extensional structures also developed in the western part of the Tabei Rise. E–E′ profile (Figs. 3, 9) is a nearly N–S-directed 3D seismic profile in the west end of the Luntai Uplift (I2 in Fig. 3). It reveals that along a salt bed at the base of the Paleogene (above and close to the T8 surface in Fig. 9b) developed a distinct bedding detachment fault. Normal faults are seen below the bedding detachment fault, but only thrust faults are recognized above (Fig. 9b). The thrust faults are likely the derivative faults of the bedding detachment fault. The
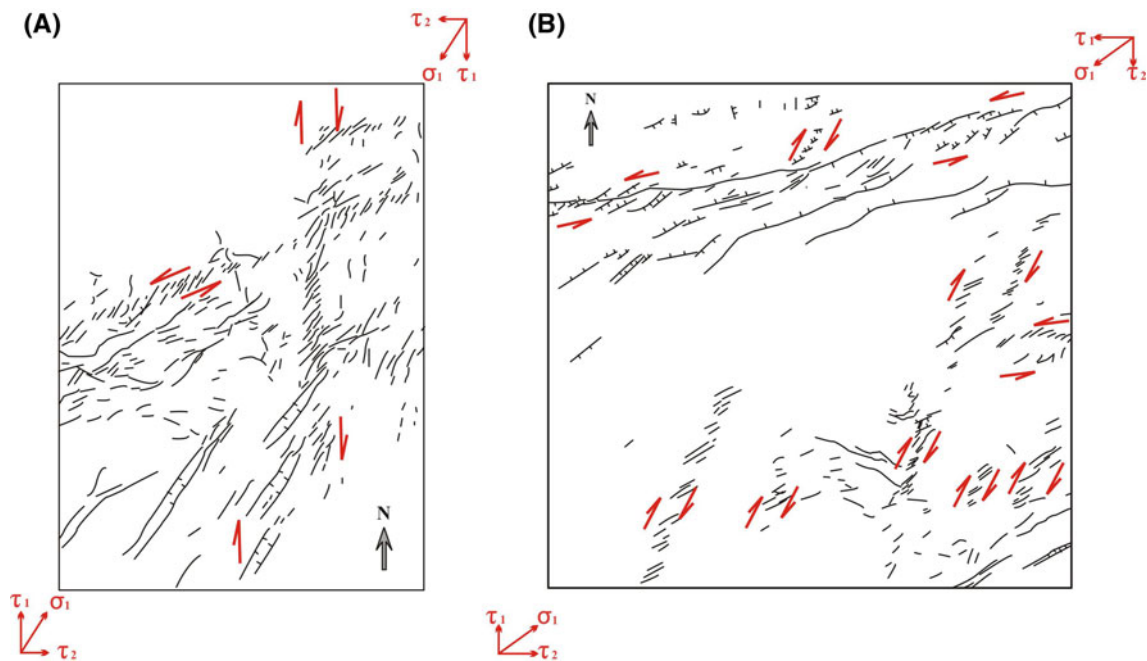
Fig. 10 Tectonic stress analysis of extensional structures: **a** the Jurassic-Early Cretaceous stage and **b** the Late Cretaceous-Neogene stage (locations shown in Fig. 3). Pairs of parallel opposite *red arrows* indicate the directions of transtensional stresses

normal faults below are truncated by the bedding detachment fault (Fig. 9b). It is not clear if the normal faults cut the strata above the detachment fault. Therefore, the complete evolution of the normal faults cannot be directly delineated; however, the evolution process can be analyzed through the determination of the upper and lower time limits of the evolution of the normal faults.

The normal faults disconnect the T8-2 and T8 surfaces, and the thicknesses of the Cretaceous on the throw side and uplift side are the same (Fig. 9b) with a growth index of 1; therefore, the extension did not occur in Cretaceous. The normal faults were formed likely after the deposition of Cretaceous. Then, when did the normal faulting stop?

The normal faults are truncated by the bedding detachment fault along the Paleogene salt bed; therefore, the bedding detachment fault and associated thrust faults certainly formed later than the formation of the normal faults. The timing of the formation of the bedding detachment faults and its associated thrust faults may define the upper limit of the formation time of the normal faults.

Determination of the formation time of the bedding detachment fault is based on its derived faults and folds. Along the E–E′ profile (Fig. 9), Ta is a reflection surface within the Neogene Jidik Formation, and the Ta surface deforms at the same pace as the strata between Ta and the bedding detachment fault, including the detachment anticline and thrust faults. The fault displacements of the thrust faults below Ta are the same, implying that below Ta, the strata thicknesses on two sides of the thrust faults are equal (Fig. 9b) and the thrust faulting did not exist. Above Ta,

the detachment folds are gradually being suppressed and finally disappeared and the fault displacements of the thrust faults also reduce gradually to zero and the faults finally vanished. The highest disconnected stratigraphic level is in the upper part of the Kangcun Formation (Table 1, Fig. 9b). Based on the above analysis, it is certain that the formation time of the bedding detachment fault and thrust faults is in the middle-early stage of Neogene Jidik Formation, and the extension likely ended before this stage.

It can be concluded that the normal faults along the E–E′ profile were formed in Paleogene and remained active up till Early Neogene. However, these Late Cretaceous-Neogene normal faults were reversed by the development of the Late Cenozoic South Tianshan fold-thrust belt.

The above detailed interpretation of seismic profiles clearly shows that the formation and evolution time of the Meso-Cenozoic extensional structures in the area can be divided into two stages. The first stage comprises the normal faults formed in the Jurassic-Early Cretaceous, mainly found in the eastern part of the Lunnan Lower Uplift and represented by A–A′ and B–B′ profiles. The normal faults in the later stage, that is, the Late Cretaceous-Neogene, are widely distributed in the Tabei Rise except in the eastern part of the Lunnan Lower Uplift.

Structural stress analysis

In the study region, there are four groups of normal fault zones, trending NS, ENE, NNE and nearly EW, and can be

further grouped into two fault systems by the formation and evolution times of the fault zones and by the characteristics, structural style, and combination relation of the faults. The left-lateral transtensional fault zone trending ENE (represented by A–A′ profile) and the right-lateral transtensional fault zone trending nearly NS (represented by B–B′ profile) are a pair of conjugate fault zones and constitute a fault system formed in the Jurassic-Early Cretaceous (Fig. 10a). The right-lateral transtensional fault zone trending NNE (represented by C–C′ profile) and the left-lateral transtensional fault zone trending nearly EW form another pair of conjugate fault zones and constitute another fault system appeared in the Late Cretaceous-Neogene (Fig. 10b). Structural stress analysis of the two normal fault systems is given below.

The Jurassic-Early Cretaceous extensional structures are mainly distributed in the eastern part of the Lunnan Lower Uplift (I1 in Fig. 3), their regional distribution comprises a series of small normal faults gathering into several nearly NS and ENE trending en echelon fault zones (Fig. 10a). The transtensional fault zone trending nearly NS was generated by right-lateral shearing, and the transtensional fault zone trending ENE was formed by left-lateral shearing, and together, they constitute a set of conjugate fault systems. The direction of the maximum principal

compressional stress σ1 of the system is NNE–SSW (Fig. 10a). The corresponding direction of the minimum principal tensile stress σ3 is WNW–ESE, indicating that during the Jurassic-Early Cretaceous, the study region was under the control of extension in WNW–ESE direction. σ1 can be decomposed into two shear stresses, in which the NS shear stress τ1 is obviously larger than the EW one τ2, implying that the study region had undergone a right-lateral shearing in N–S direction (Fig. 10a).

The Late Cretaceous-Neogene extensional structures are widely seen in the Tabei Rise (I in Fig. 3). A series of normal faults occur regionally in en echelon and can be divided into nearly NNE and ENE trending normal fault zones (Fig. 10b). The nearly NNE trending transtensional fault zone generated by right-lateral shearing together with the ENE-directed transtensional fault zone formed by left-lateral shearing constitute another conjugate fault system (Fig. 10b). The direction of maximum principal compressional stress σ1 is NE–SW and the direction of corresponding minimum principal tensile stress σ3 is NW–SE, suggesting that the study region was extended in NW–SE direction during the Late Cretaceous-Neogene. The σ1 can be decomposed into two shear stresses. The NS shear stress τ2 is smaller than the τ1 on EW direction (Fig. 10b), implying that the study region had undergone a left-lateral shearing in E–W direction.
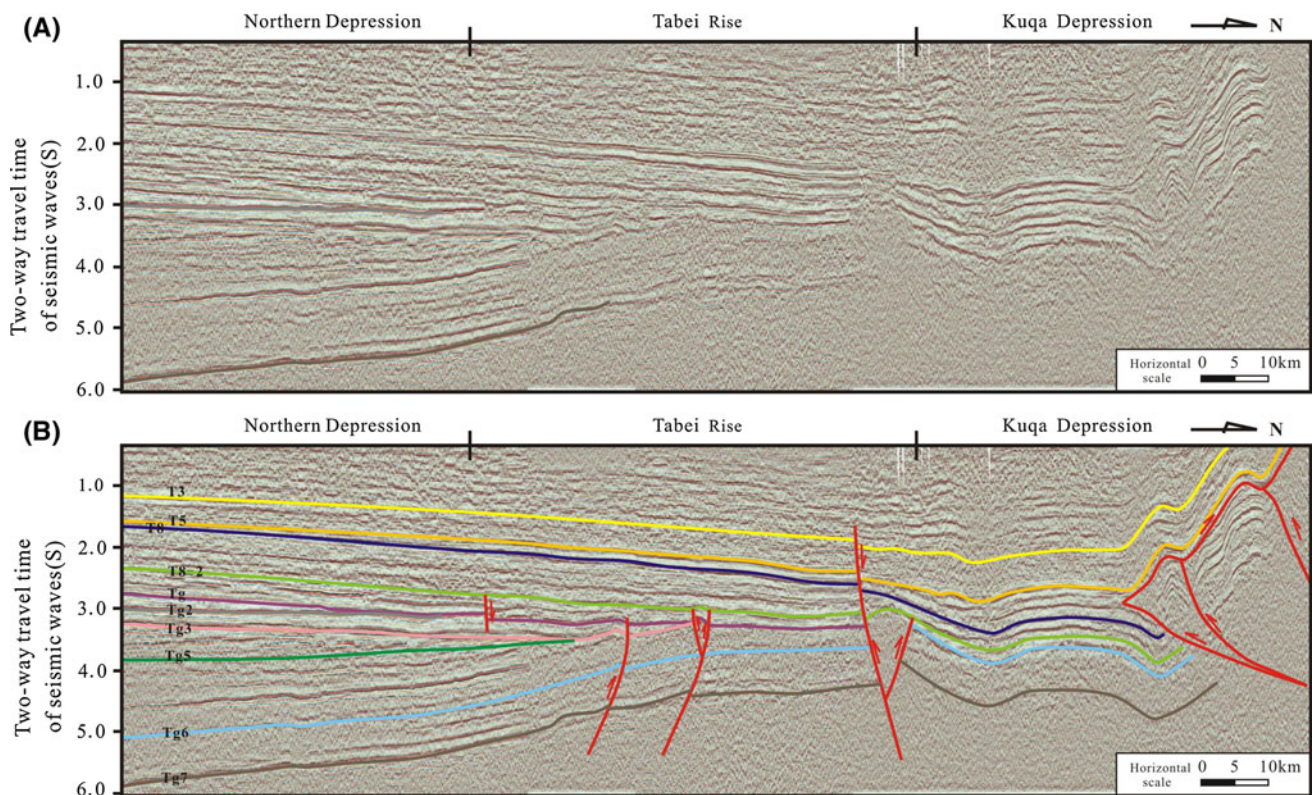

Fig. 11 The N–S-directed TLM-Z50 seismic profile crossing the Tabei Rise. The *upper one* is original and the *lower* interpreted (code number of seismic reflection surface shown in Table 1)

Discussion

As described above, the postulated origins of the Meso-Cenozoic extensional structures are in conflict with several other tectonic postulations in the area. For example, is it possible that these extensional structures were resulted from the longitudinal tension at arched area of compressional anticlines in the forebulge of Kuqa peripheral foreland basin? What is the relationship between the Jurassic-Early Cretaceous extensional structures and the widely distributed Jurassic coal measures in the South Tianshan? If the Meso-Cenozoic extensional structures truly exist, then why it is not able to be observed in the field? These problems will be discussed separately below.

Relationship of the Meso-Cenozoic extensional structures in the Northern Tarim Basin to the forebulge of the Kuqa peripheral foreland basin

Previous studies suggested that the Meso-Cenozoic extensional structures in the Tabei Rise were resulted from longitudinal tension at arched area of compressional anticlines in the forebulge of the Kuqa foreland basin (Tang et al. 1999; Tang and Jin 2000; Wei et al. 2001).

Large anticlines in the Tabei Rise were formed in late-Early Paleozoic and evolved in Late Paleozoic, and finally set as the forebulge of Kuqa foreland basin in the terminal Permian–Triassic (Fig. 11b). The formation and evolution time of these anticlines obviously did not match with that of the Meso-Cenozoic extensional structures. Regional seismic profiles crossing the Tabei Rise (Fig. 11) reveal that, during the development of the Meso-Cenozoic extensional structures (J–N), no large anticlines occurred in the Tabei Rise (Fig. 11). In addition, new seismic data indicate that the Meso-Cenozoic extensional structures are not limited to the arched area of the Tabei Rise (Fig. 3). Therefore, the origin of Meso-Cenozoic extensional structures in the region cannot be adequately explained by the local extensional structural stress field created by the local longitudinal extension at the arched area of the Kuqa forebulge foreland basin.

Genesis of the Jurassic-Early Cretaceous extensional structures

The Jurassic-Early Cretaceous normal faults demonstrate likely a regional extensional tectonic background. Besides the normal faults, the widely distributed Jurassic coal measures are also an important evidence of the regional extensional structures (Bureau of Geology and Mineral Resources of Xinjiang Uygur Autonomous Region 1993; Wang et al. 2011; Wu et al. 1999). Jia et al. (2001) when studying the oil and gas basins in North Tethys have suggested that after the terminal Triassic-Early Jurassic

collisional orogeny, isostatic adjustments in the Cimmerian orogenic belt would induce post-orogenic extension and put the orogenic belt as well as the neighboring areas into an extensional tectonic environment, and enable the formation of the Jurassic normal faults in the Tarim Basin. In addition, Chen et al. (2009) discover the Early Jurassic extensional structures in Southeast Tarim Basin and postulated that they were resulted from the post-orogenic stress relaxation of collisional orogeny between the Qiangtang terrane and Laurasia continent.

We also propose that the Jurassic-Early Cretaceous extensional structures in the Tarim Basin were resulted from the post-orogenic relaxation in the North Tethys. However, the difference is that we postulate that not only the post-orogenic relaxation of the Cimmerian orogen but also the post-orogenic relaxation of the South Tianshan orogen may be an important element in the formation of the Jurassic-Early Cretaceous extensional structures. This is because (1) the post-orogenic relaxation of Cimmerian orogen cannot reasonably reconcile the origin of all the Jurassic-Early Cretaceous extensional structures in the Tarim Basin. The Cimmerian collisional orogeny took place at the terminal Triassic-Early Jurassic (Jia et al. 2001); however, the formation of the Jurassic-Early Cretaceous normal faults in Northern Tarim started out at the terminal Triassic-Early Jurassic (and some seismic profiles even indicate that the normal faults may have happened at terminal Triassic) (Figs. 5, 6). Therefore, there is a time discrepancy. (2) Previously, the South Tianshan collision event was thought to take place in the Middle or even Early Paleozoic (Wang et al. 1990; Shu et al. 2007; Gao et al. 1995; Laurent-Charvet et al. 2002, 2003; Charvet et al. 2007); however, updating geologic evidences, including data from paleontology, isotopic chronology, mineral deposit geology, petrology and lithogeochemistry, and from studies on the South Tianshan indicate that the South Tianshan paleo-ocean was not completely closed at the terminal Permian. The time of the complete closure and the South Tianshan collision event likely happened in the terminal Permian–Triassic (Long et al. 2006; Han et al. 2006; Zhang et al. 2005, 2007; Xiao et al. 2004, 2008, 2009, 2012; Li et al. 2001a, b, 2002, 2003, 2005, 2009, 2010). This new point of view reconciles the temporal relationship with the formation time of the Jurassic-Early Cretaceous normal faults in the Tarim Basin. Therefore, it is believed that the formation of the Jurassic-Early Cretaceous normal faults in the Tarim Basin was not only related to the post-orogenic stress relaxation of the Cimmerian orogenic belt but also controlled by the post-orogenic stress relaxation of the South Tianshan orogenic belt. The Jurassic-Early Cretaceous normal faults in the Northern Tarim Basin likely have closer relationship with the post-orogenic stress relaxation of the South Tianshan orogenic belt.
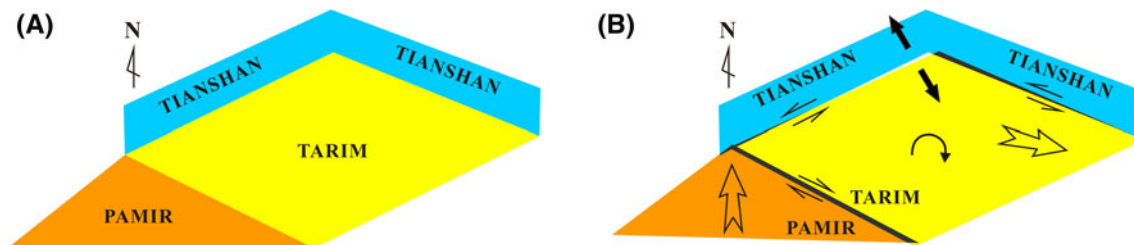
Fig. 12 A cartoon showing the origin of the Late Cretaceous-Neogene extensional structures: **a** before the deformations and **b** after the deformations. The *narrow black strips* in (**b**) represent compressional areas and the white strips extensional area. The *blank arrows* show the northerly wedging direction of Pamir and the east by south escape direction of the Tarim relative to the South Tianshan. The *black arrows* indicate extensional direction in the Northern Tarim and the *semicircle arrow* shows the clockwise rotation direction of the Tarim relative to the South Tianshan

Stress analysis reveals that the Jurassic-Early Cretaceous extensional structures in the Northern Tarim Basin exhibit a slight anticlockwise rotation relative to the South Tianshan. We also noticed that previous paleomagnetic data indicate that the Tarim block kept rotating clockwise in millions of years in Phanerozoic (Fang et al. 1996). How can the difference be accounted for? First of all, we have to emphasize the difference in the basic concepts between the two rotations. In paleomagnetic study, the rotation of the Tarim block means that the block was rotated with respect to the (present) longitude and latitude of the Earth; however, the rotation in this paper means only a rotation of the Northern Tarim relative to the South Tianshan. These two kinds of rotations do not have direct relationship and therefore are not in contradiction. Second, the block rotation revealed by paleomagnetic method is generally a rough estimate on a large scale; however, the rotation revealed in our study is on a small and fine scale and likely beyond the resolution of paleomagnetic measurement. Third, the features of structures revealed in our paper, though on a small scale, will likely be helpful in future paleomagnetic study on the Tarim Basin.

Our study on the Meso-Cenozoic extensional structures in the Northern Tarim Basin indicates that the Meso-Cenozoic extensional structures and their origin are complicated and more work needs to be done in the future.

Origin of the Late Cretaceous-Neogene extensional structures

The time of the development of Late Cretaceous-Neogene extensional structures likely coincides with the time of the Himalayan collisional orogeny (Gansser 1991; Beck et al. 1995; Xiao et al. 1988; Liu et al. 1993; Xu et al. 1993a, b; Li et al. 2000). Central Asia was then under the control of a regional compressional tectonic field. Obviously, the origin of the Late Cretaceous-Neogene extensional structures cannot be explained by an inexistent regional extensional field but likely by a kind of block escape and rotation under the regional compressional tectonic background. The escape direction of the Tarim block was likely east by south and accompanied by a certain degree of clockwise rotation relative to the South Tianshan (Fig. 12).

The regional tectonics in Central Asia was extensional since the Jurassic, but the far-field effect of the Himalayan orogeny transformed it into a regional compressional tectonic regime. Under this compressional tectonic background, strong compressional thrusting happened in Central Asia. In the meantime, tectonic adjustment among different blocks may trigger tectonic escapes and rotations. The possible east by south escape of the Tarim block relative to the South Tianshan likely created a local extensional structural stress field in the study area (Fig. 12b). Furthermore, relative to the South Tianshan, the Tarim block likely rotated clockwise and induced the left-lateral transtensional fault zone. Similar transtensional fault structures were reported in the southeast of the Qinghai-Tibet Plateau (Harrison et al. 1996). The collision between India and Asia as well as the induced block escape had long been taken seriously (Xiao et al. 1988; Molnar and Tapponnier 1975; Tapponnier and Molnar 1977; Tapponnier et al. 1982, 1986). The escape of cratonic blocks (including North China and Yangtze) was realized by shear slip between adjacent blocks. The escape of the Tarim block in the Late Cretaceous-Neogene was likely a part of the activities. Avouac and Tapponnier (1993) had inferred the clockwise rotation of the Tarim block when they studied the active tectonics in Central Asia. Our study likely verifies the inferred clockwise rotation proposed by Avouac and Tapponnier (1993).

The Late Cretaceous-Neogene extensional structures in the Northern Tarim are likely a good example of extensional structures occurred in a relatively limited area located in a setting of regional compressional tectonics.

Difficulty in field observation for the Meso-Cenozoic extensional structures in Tarim Basin and its periphery

Why the Meso-Cenozoic normal faults were not recognized through field geological observation in the Tarim Basin and its periphery? First of all, the peripheral

mountains of the Tarim Basin were formed by the massive tectonic uplift during the Himalayan collisional orogeny; in which the strong compressional thrusting modified intensively all earlier deformations. Except ductile deformation, early brittle deformations (including the Meso-Cenozoic normal faults) were almost completely modified, and therefore, difficult to be recognized, though scanty traces may have been left. Secondly, Meso-Cenozoic rocks are mainly developed in the basin but covered by the Quaternary desert/gobi. Therefore, the Meso-Cenozoic rocks and the related normal faults are difficult to be observed on the surface. Thirdly, outcrops in the area are mainly pre-Mesozoic with a few Mesozoic-Neogene; therefore, the possibility of discovering the Meso-Cenozoic extensional tectonics on the surface is further reduced.

Conclusions

In the Northern Tarim Basin, the Meso-Cenozoic extensional structures are widely developed. A series of small normal faults regionally arrange in left- or right-step en echelon and constitute several transtensional fault zones. In profile, they group into graben-horst structures and staircase-like normal fault combinations.

Four groups of Meso-Cenozoic en echelon transtensional fault zones are revealed, trending nearly NS, ENE, NNE, and nearly EW. They combine into two conjugate normal fault systems: one comprises a nearly NS trending left-step right-lateral transtensional fault zone and a ENE trending right-step left-lateral transtensional fault zone; the other consists of a nearly NNE trending left-step right-lateral transtensional fault zone and an EW trending right-step left-lateral transtensional fault zone. The two systems represent separately the extensional structures formed in the Jurassic-Early Cretaceous stage and Late Cretaceous-Neogene stage.

The Jurassic-Early Cretaceous extensional structures are part of the North Tethys Mesozoic extensional structures. They likely linked closely to the stress relaxation immediately after the South Tianshan collisional orogeny and accompanied by a weak anticlockwise rotation of the Tarim block relative to the South Tianshan.

The Late Cretaceous-Neogene extensional structures were likely resulted from the mass escape with a certain degree of rotation triggered by the far-field effect of the Himalayan collisional orogeny. Relative to the South Tianshan, the escape direction of the Tarim Block was east by south with a certain degree of clockwise rotation.

References

Allen MB, Vincent SJ, Wheeler PJ (1999) Late Cenozoic tectonics of the Kepingtage thrust zone: interactions of the Tien Shan and Tarim Basin, northwest China. Tectonics 18:639–654

Avouac JP, Tapponnier P (1993) Kinematic model of active deformation in Central Asia. Geophys Res Lett 20:895–898

Beck RA, Burbank DW, Sercombe WJ, Riley GW, Barndt JK, Berry JR, Afzal J, Khan AM, Jurgen H, Metje J, Cheema A, Shafique NA, Lawrence RD, Khan MA (1995) Stratigraphic evidence for an early collision between northwest India and Asia. Nature 373:55–58

Bullen ME, Burbank DW, Garver JI (2001) Late Cenozoic tectonic evolution of the northwestern Tien Shan: new age estimates for the initiation of mountain building. Geol Soc Am Bull 113:1544–1559

Bureau of Geology and Mineral Resources of Xinjiang Uygur Autonomous Region (1993) Regional Geology of Xinjiang Uygur Autonomous Region. Geological Publishing House, Beijing, pp 1–841 (in Chinese)

Charvet J, Shu L, Laurent-Charvet S (2007) Paleozoic structural and geodynamic evolution of eastern Tianshan (NW China): welding of the Tarim and Junggar plates. Episodes 30:162–185

Chen CM, Lu HF, Jia D, Xie XA (1998) Neogene-Quaternary sedimentary features and structural deformation of the Tarim Basin and its petroleum geological significances. Acta Sediment Sin 16:113–116 (in Chinese with English abstract)

Chen HL, Luo JC, Guo QY, Liao L, Xiao ZY, Cheng XG, Yang SF, Wang BQ (2009) Deformation history and tectonic evolution of the Southeastern Tarim Basin in Mesozoic and Cenozoic. Geotecton Metallog 33(1):38–45 (in Chinese with English abstract)

Fang DJ, Tan XD, Jiang LP, Wang PY (1996) Phanerozoic paleomagnetism of the Northern Tarim Basin. In: Tong XG, Liang DG, Jia CZ (eds) New advance in petroleum geologic research in the Tarim Basin. Scientific Press, Beijing, pp 196–205 (in Chinese with English abstract)

Gansser A (1991) Facts and theories on the Himalayas. Ecol Geol Helv 84:33–60

Gao J, He GQ, Li MS, Xiao XC, Tang YQ (1995) The mineralogy, petrology, metamorphic PTDt trajectory and exhumation mechanism of blueschists, the South Tianshan, Northwestern China. Tectonophysics 250:151–168

Guo LZ, Shi YS, Lu HF (1992) Two kinds of long distance effect by collision of Indian and Qingzang tectonic plate. In: Li QB, Dai JX, Liu RQ, Li JL (eds) Symposium of the researches on modern geology [volume I]. Nanjing University Press, Nanjing, pp 1–8 (in Chinese)

Han CM, Xiao WJ, Zhao GC, Mao JW, Li SZ, Yan Z, Mao QG (2006) Major types, characteristics and geodynamic mechanism of Late Paleozoic copper deposits in the Northern Xinjiang, Northwestern China. Ore Geol Rev 28:308–328

Harrison TM, Leloup PH, Ryerson FJ, Tapponnier P, Lacassin R, Chen W (1996) Diachronous initiation of transtensional along

the Ailao Shan-Red River Zone, Yunnan and Vietnam. In: Yin A, Harrison TM (eds) The tectonic evolution of Asia. Cambridge University Press, Cambridge, pp 205–226

Jia CZ, Yao HJ, Gao J, Zhou DY, Wei GQ (1992) Stratigraphic system of the Tarim Basin. In: Tong XG, Liang DG (eds) Symposium of the oil and gas exploration in the Tarim Basin. Xinjiang Technology and Medical Publishing House, Urumqi, pp 34–63 (in Chinese)

Jia D, Lu HF, Cai DS, Chen CM (1997) Structural analyses of Kuqa foreland fold-thrust belt along the northern margin of the Tarim Basin. Geotecton Metallog 21(1):1–8 (in Chinese with English abstract)

Jia CZ, Yang SF, Chen HL, Wei GQ (2001) Structural geology and natural gas of the group of basins in the northern margin of Tethyes. Petroleum Industry Press, Beijing, pp 1–162 (in Chinese)

Jia CZ, Zhang SB, Wu SZ (2004) Stratigraphy of the Tarim Basin and adjacent areas. Science Press, Beijing, pp 1–547 (in Chinese)

Laurent-Charvet S, Charvet J, Shu L, Ma R, Lu HF (2002) Paleozoic late collisional strike-slip deformations in Tianshan and Altay, Eastern Xinjiang, NW China. Terra Nova 14:249–256

Laurent-Charvet S, Charvet J, Monie P, Shu L (2003) Late Paleozoic strike-slip shear zones in eastern central Asia (NW China): new structural and geochronological data. Tectonics 22:1009

Li YJ, Chen CX, Mai GR, Zeng Q, Luo JC, Huang ZB, Zheng DM, Peng GX (2000) Dual foreland basin model of continent–continent collision orogenic belt: evidence from Dabieshan, Himalayan and Uralian orogenic belts. Acta Geosci Sin 21(1):7–16 (in Chinese with English abstract)

Li YJ, Li YP, Wu HR, Hu JF, Su YS, Huang ZB (2001a) Radiolarian fossils discovered from the chert gravels of Triassic conglomerate at the NW margin of the Tarim Basin, NW China, and discussions. Sci Geol Sin 10(4):275–282

Li YJ, Song WJ, Mai GR, Zhou LX, Hu JF, Shang XL (2001b) Kuqa foreland basin, Northern Tarim foreland basin and their coupling relationship. Xinjiang Pet Geol 22(5):376–381 (in Chinese with English abstract)

Li YJ, Wang ZM, Wu HR, Huang ZB, Tan ZJ, Luo JC (2002) Discovery of Radiolarian Fossils from Aiktik Group at the Western end of the Southern Tianshan Mountains of China and its implications. Acta Geol Sin 76(2):146–154

Li JY, Xiao WJ, Wang KZ, Sun GH, Gao LM (2003) Neoproterozoic–Paleozoic tectonostratigraphic framework of Eastern Xinjiang, NW China. In: Mao JW, Goldfarb R, Seltmann R, Wang DH, Xiao WJ, Hart C (eds) Tectonic evolution and metallogeny of the Chinese Altay and Tianshan. IGCP 473 workshop 2003, Urumuqi, international association on the genesis of ore deposits (IAGDO), CERAMS, Natural History Museum, London, pp 31–74

Li YJ, Sun LD, Wu HR, Wang GL, Yang CS, Peng GX (2005) Permo-carboniferous radiolaria from the Wupatarkan group, west terminal of Chinese south Tianshan. Chin J Geol 40(2):220–226 (in Chinese with English abstract)

Li YJ, Wu GY, Lei GL, Zhang JZ, Wang YR, Liu YL (2008) Deformational features, ages and mechanism of the Cenozoic Kuqa foreland fold-and-thrust belt in Xinjiang. Chin J Geol 43(3):488–506 (in Chinese with English abstract)

Li YJ, Yang HJ, Zhao Y, Luo JC, Zheng DM, Liu YL (2009) Tectonic framework and evolution of the South Tianshan, NW China. Geotecton Metallog 33(1):96–106 (in Chinese with English abstract)

Li YJ, Zhang HA, Qian YX, Zhang QR, Zhao Y, Liu YL (2010) The collision time of the South Tianshan orogen, NW China. Chin J Geol 45(1):57–65 (in Chinese with English abstract)

Liu BJ, Yu GM, Xu Q (1993) Formation and evolution of the Mesozoic and Cenozoic deep-water sedimentary basins along the Yarlung Zangbo river (I): sedimentary characteristics and evolution of the Himalayan orogenic zone. Sediment Geol Tethyan Geol 13(1):32–49 (in Chinese with English abstract)

Liu ZH, Lu HF, Li XJ (2000) Tectonic evolution of Kuqa rejuvenated foreland basin. Chin J Geol 35(4):482–492 (in Chinese with English abstract)

Long LL, Gao J, Xiong XM, Qian Q (2006) Geochemical characteristics and age of the Kule Lake ophiolite in the Southern Tianshan. Acta Petrol Sin 22(1):65–73 (in Chinese with English abstract)

Lu HF, David GH, Jia D, Cai DS, Wu SM, Chen CM, Shi YS, Zenon CV (1994) Rejuvenation of the Kuqa foreland basin, northern flank of the Tarim Basin, northwest China. Int Geol Rev 36: 1151–1158

Lu HF, Chen CM, Liu ZH, Jia D, Wang GQ, Jia CZ (2000) The structural features and origin of the Kuqa rejuvenation foreland thrust belt. Acta Petrol Sin 21(3):19–24 (in Chinese with English abstract)

Meng QL, Li YJ, Shi J, Jing B, Feng XJ, Zhao Y (2008) Main characters and active ages of the Selibuya Kangxi faults in the Western Tarim Basin. Chin J Geol 43(2):282–293 (in Chinese with English abstract)

Molnar P, Tapponnier P (1975) Cenozoic tectonics of Asia: effects of a continental collision. Sci New Ser 189:419–426

Scharer KM, Burbank DW, Chen J (2004) Detachment folding in the Southwestern Tian Shan-Tarim foreland, China: shortening estimates and rates. J Struct Geol 26:2119–2137

Shu LS, Wang B, Zhu WB (2007) Age of Radiolarian Fossils from the Heiyingshan ophiolitic mélange, Southern Tianshan Belt, NW China, and its tectonic significance. Acta Geol Sin 81(9):1161–1168 (in Chinese with English abstract)

Sobel ER, Dumitru TA (1997) Thrusting and exhumation around the margins of the western Tarim Basin during the India–Asia collision. J Geophys Res 102:1043–1063

Sun LD, Li YJ, Song WJ, Tian ZJ, Wang GL, Wu GH (2002) Tectonics and oil-gas distribution in the North Tarim Basin, NW China. Chin J Geol 37:1–13 (in Chinese with English abstract)

Tang LJ, Jin ZJ (2000) Negative inversion process and hydrocarbon accumulation of Yaha Fault Belt in the Northern Uplift, Tarim Basin. Acta Sediment Sin 18(3):302–309 (in Chinese with English abstract)

Tang LJ, Jin ZJ, Zhang YW, Lu KZ (1999) Negative inversion structures and geological significance of the Northern Uplift, the Tarim Basin, northwestern China. Geosciences 13(1):93–98 (in Chinese with English abstract)

Tang LJ, Jin ZJ, Jia CZ, Pi XJ, Chen SP, Xie HW, Wang ZY (2004) A large-scale salt nappe complex in the leading edge of the Kuqa foreland fold-thrust belt, Tarim Basin, Northwest China. Acta Geol Sin 43(2):17–25 (in Chinese with English abstract)

Tapponnier P, Molnar P (1977) Active faulting and tectonics in China. J Geophys Res 82:2095–2930

Tapponnier P, Peltzer G, Le Dain AY, Armijo R, Cobbold P (1982) Propagating extrusion tectonics in Asia: new insights from simple experiments with plasticine. Geology 10:611–616

Tapponnier P, Peltzer G, Armijo R (1986) On the mechanics of the collision between India and Asia. Geol Soc Lond Special Publ 19:113–157

Wang RD (1992) New progress of seismic geologic stratum division and calibration in the Tarim Basin. In: Tong XG, Liang DG (eds) Symposium of oil and gas exploration in the Tarim Basin. Xinjiang Technology and Medical Publishing House, Urumqi, pp 131–141 (in Chinese)

Wang ZX, Wu JY, Liu CD, Lu XC, Zhang JG (1990) Polycyclic Tectonic evolution and Metallogeny of the Tianshan Mountains. Science Press, Beijing, pp 1–217 (in Chinese with English abstract)

Wang X, Jia CZ, Yang SF (2002) Geometry and kinematics of the Kuqa fold-and-thrust belt in the Southern Tianshan. Chin J Geol 37(3):372–384 (in Chinese with English abstract)

Wang GL, Li YJ, Sun JH, Huang ZB, Zhao Y, Liu YL (2009) Structural deformation characteristics of the Kalpin thrust belt, NW Tarim. Chin J Geol 44(1):50–62 (in Chinese with English abstract)

Wang SE, Ye LS, Guo XP (2011) Jurassic strata, palaeoenvironment and oil-gas resources in the Tianshan tectonic belt, Xinjiang, China—taking the Kümüx basin as an example. Geol Bull Chin 30(2/3):410–417 (in Chinese with English abstract)

Wei GQ, Jia CZ, Shi YS, Lu HF, Li YH (2001) Tectonic characteristics and petroleum accumulation in extensional-shear fault system in Mesozoic-Cenozoic formations in the northern area of the Tabei Uplift, Tarim. Acta Petrol Sin 22(1):19–24 (in Chinese with English abstract)

Wu FQ, Wang M, Qin WJ, Li YL, Ma Q, He YB (1999) Triassic-Jurassic petroleum system in the Yanqi Basin. Pet Explor Dev 26(5):5–7 (in Chinese with English abstract)

Xiao XC, Li TD, Li GQ (1988) Tectonic and evolution of the himalayan lithosphere. The Geological Publishing House, Beijing, pp 1–57 (in Chinese)

Xiao WJ, Zhang LC, Qin KZ, Sun S, Li JL (2004) Paleozoic accretionary and collisional tectonics of the Eastern Tianshan (China): implications for the continental growth of central Asia. Am J Sci 304:370–395

Xiao WJ, Han CM, Yuan C, Sun M, Lin SF, Chen HL, Li ZL, Li JL, Sun S (2008) Middle Cambrian to Permian subduction-related accretionary orogenesis of Northern Xinjiang, NW China: implications for the tectonic evolution of central Asia. J Asian Earth Sci 32:102–117

Xiao WJ, Windley BF, Huang BC, Han CM, Yuan C, Chen HL, Sun M, Sun S, Li JL (2009) End-Permian to mid-Triassic termination of the accretionary processes of the southern Altaids: implications for the geodynamic evolution, Phanerozoic continental growth, and metallogeny of Central Asia. Int J Earth Sci 98:1189–1217

Xiao WJ, Windley BF, Allen M, Han CM (2012) Paleozoic multiple accretionary and collisional tectonics of the Chinese Tianshan orogenic collage. Gondwana Research. doi:10.1016/j.gr.2012.01.012

Xu Q, Liu BJ, Yu GM (1993a) Formation and evolution of the Mesozoic and Cenozoic deep-water sedimentary basins along the Yarlung Zangbo river (II): dynamics of the Himalayan carbonate platforms. Sediment Geol Tethyan Geol 13(1):50–57 (in Chinese with English abstract)

Xu Q, Liu BJ, Yu GM (1993b) Formation and evolution of the Mesozoic and Cenozoic deep-water sedimentary basins along the Yarlung Zangbo river (III): tectonic subsidence of the Himalayan passive continental margins. Sediment Geol Tethyan Geol 13(1):58–65 (in Chinese with English abstract)

Yang HJ, Li YJ, Shi J, Xiao AC, Huang SY, Wu GY, Wang HS, Wang X, Zhao Y, Liu YL (2010) Tectonic characteristics of the Late Cenozoic South Tianshan fold-thrust belt. Quat Sci 30(5):1030–1043 (in Chinese with English abstract)

Yin A, Nie S, Craig P, Harrison TM (1998) Late Cenozoic tectonic evolution of the South Chinese Tian Shan. Tectonics 17(1):1–27

Zhang PZ, Deng QD, Yang XP, Peng SZ, Xu XW (1996) Late Cenozoic tectonic deformation and mechanism along the Tianshan mountain, Northwestern China. Earthq Res Chin 12(2):127–140 (in Chinese with English abstract)

Zhang LF, Song SG, Liou JG, Ai YL, Li X (2005) Relict coesite exsolution in omphacite from the Western Tianshan eclogites, China. Am Miner 90:181–186

Zhang LF, Ai YL, Li XP, Rubatto D, Song B, Williams S, Song SG, Liou JG (2007) Triassic collision of the Western Tianshan orogenic belt, China: evidence from SHRIMP U-Pb dating of zircon from HP/UHP eclogitic rocks. Lithos 96:266–280

Zheng M, Lei GL, Huang SY, Wu C, Luo SC, Li YJ (2007) Features of fault structure in the southern margin of west segment of the south Tianshan, and its control to the evolution of the Wushi sag. Chin J Geol 42(4):639–655 (in Chinese with English abstract)

Zheng M, Meng ZF, Luo SC, Feng XJ, Jing B, Li Y, Li YJ (2009) Tectonic evolution series of the Niaoshan structure belt in the Bachu uplift, Tarim Basin, and its significance in hydrocarbon exploration. Acta Geol Sin 83(1):16–24 (in Chinese with English abstract)